Modeling and aeroelastic investigation of the A3TB

Noam Yechieli
Advisor: Prof. Daniella E. Raveh
Technion Israel institute of technology

December 7, 2019

Abstract

The report presents a study of the aeroelastic stability of a flexible flying wing configuration that is currently under development. The Active Aeroelastic Aircraft Testbed (A3TB) has been developed in a student project, as a part of the first year of a 3-years project. The wing, like other flying wing configurations, is prone to flutter in a body freedom flutter mechanism. Towards the aeroelastic investigation, a finite element model was constructed for the clamped wing and was used for free vibration analysis. The model has been updated and refined through static loading and ground vibration tests. Based on the modal model, a flutter analysis was carried out to predict the flutter speed and flutter mechanism. For this analysis, the ZAERO software by ZONA technologies was used. The results have shown a flutter speed lower than expected. Current stability analyses target the free aircraft configuration.

I. Introduction

Over the last several years, there has been a growing interest in the aeroelastic behavior of very flexible planes[2]. Hence, there were also attempts to study it in the Technion's faculty of aerospace engineering, and therefore the Active Aeroelastic Aircraft Testbed (A3TB) project was started. In this project, students in their last year mostly take part in developing and testing a fully functioning aircraft of their own built. The aircraft has eight control surfaces that allow it to maneuver in flight and is build mostly from 3D-printed parts from PA12 nylon. During its development, there were some important missions to accomplish while designing it, one of them was aeroelastic stability analysis, which is the one presented in this report. Naturally, the flying wing configuration has low pitch inertia, thus the short period mode has a relatively high frequency. Because of the flexibility of the structure, it has a low first bending mode frequency. Due to the flying wing configuration of the aircraft, there was a concern regarding its vulnerability to body freedom flutter (BFF) [1]. BFF is a phenomenon common to aircraft which have a similar frequency range of the flight dynamics and aeroelastic response. It may appear in the coupling of the first bending frequency with the short period rigid body mode. Flutter occurs where the first wing bending mode or the short period loses stability. The SC005 SensorCraft [2] swept flying wing designed by Lockheed-Martin was a similar configuration that was examined for Body Freedom Flutter and a passive and active means to mitigate it. Another study on flutter suppression in a flying wing configuration aircraft was NASA and Lockheed Martin's X-56 platform [4]. The control loop had to have a high control frequency to avoid dynamic coupling between the structure and the control law. The control law had a frequency of about one order of magnitude higher than the structural modes that were taken into account [3]. The findings of this research indicated that passive means can only mitigate flutter with a small efficiency and might cause unnecessary weight addition or other abnormalities that are unwanted at the design level. This report presents the aeroelastic investigation of the A3TB aircraft. In the first part, the finite element (FEM) model construction is shown, with the free vibration analysis results. The second part presents the flutter investigation of the aircraft and the tests which followed.

II. Mathematical Model

Flutter calculation using modal approach:
The aeroelastic equations of motion (EOM) in the physical coordinates can be written as:

$$[M]\{\ddot{q}\} + \Big([K] - \rho v^2 [A(ik)]\Big)\{q\} = \{0\} \tag{1}$$

Where M is the mass matrix,K is the stiffness matrix, and $[A(ik)]$ is the aerodynamic influence coefficient matrix which is dependent on the reduced frequency k, defined as: $k = \frac{\omega b}{v}$.

Using the modal approach, the physical desplacements can be written as a combination of a few low-frequency modes:

$$\{q\} = [\phi]\{\xi\} \tag{2}$$

Where $[\phi]$ is the modes matrix

$$[\phi] = [\phi_1, \phi_2, ..., \phi_N]$$

Assigning (2) into the EOM (Eq. 1), the aeroelastic EOM in generalized coordinates can be written as:

$$\overbrace{[\phi]^T [M] [\phi]}^{GM}\{\ddot{\xi}\} + \left(\overbrace{[\phi]^T [K] [\phi]}^{GK} - \rho v^2 \overbrace{[\phi]^T [A(ik)] [\phi]}^{[Q(ik)]}\right)\{\xi\} = \{0\}. \tag{3}$$

GM and GK are the generalized mass and stiffness matrices, usually normalized s.t the mass matrix is a unitary matrix, and the stiffness matrix is also diagonal with diagonal terms ${\omega_i}^2$. $[Q(ik)]$ is the generalized aerodynamic force coefficient matrix in which the i,j term is the generalized force component in the i-th degree of freedom (DOF) as a result of a unit displacement at the ξ^{th} DOF. Assuming an harmonic motion at flutter:

$$\{\xi\} = \{\xi_0\} e^{i\omega t}$$

In the k-method solution, a fictitious damping proportional to the stiffness, is added to the system to bring it to the verge of instability.

$$\Big(-\omega^2 [GM] - \rho v^2 [Q(ik)] + (1 + ig)[GK]\Big)\{\xi_0\} = \{0\} \tag{4}$$

Rearranging Eq. 4:

$$\left([GK]^{-1}\left([GM] + \frac{\rho \cdot b^2}{k^2}[Q(ik)]\right) - \lambda [I]\right)\{\xi_0\} = \{0\} \tag{5}$$

The flutter problem is posed as an eigenvalues problem:

$$([F] - \lambda [I])\{\xi_0\} = \{0\} \tag{6}$$

Where $F = [GK]^{-1}\left([GM] + \frac{\rho \cdot b^2}{k^2}[Q(ik)]\right)$.
The eigenvalues are $\lambda = \frac{1}{\omega^2} + i\frac{g}{\omega^2}$ from which the frequency, damping and velocity can be computed as: $\omega = \frac{1}{\sqrt{\mathrm{Re}(\lambda)}}$; g $= \frac{\mathrm{Im}(\lambda)}{\mathrm{Re}(\lambda)}$ and $v = \frac{\omega b}{k}$.
Flutter onset is obtained at the velocity for which g, the added fictitious damping, is zero. Assigning the value of k at flutter onset to the eigenvalue problem, Eq. 6 is solved for the

flutter vector, $\{\xi_0\}$, describing the modes participating in flutter, and their phase (complex vector). Divergence accrues when one of the modes branches loses stability, ($\xi = 0$) and the corresponding frequency is zero.
In this study, flutter onset was computed by ZAERO aeroelastic software using the k-method described above, and also by the g-method. The latter is presented in [5].

III. The A3TB model

i. Geometric model

The dimensions of the A3TB are shown in Figure 1. The aircraft has a flying wing configuration, with aspect ratio of 8.4, a chord length of 295mm. It weights 11kg, powered by an electric propulsion system, and controlled by eight trailing-edge control surfaces.

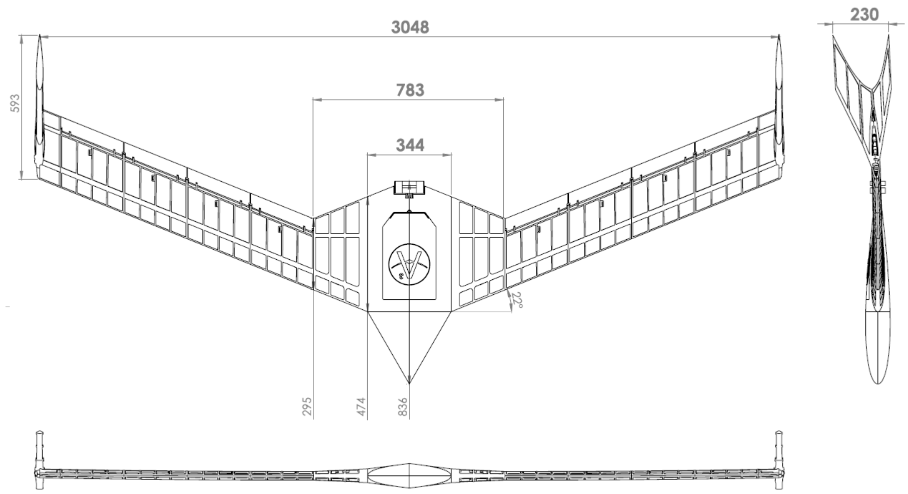

Figure 1: *Drawing of the A3TB*

The A3TB structure is constructed of a main spar carrying six separable 3D printed segments of each side, as shown in Figure 2. The main spar is a 20mmx5mm laminated carbon-fiber beam. The wing is swept back in a 22°, with a 3°washout twist, and a NACA0012 airfoil, and has wing-tip fins to increase its lateral stability.

The essential geometric and inertial data is provided in Table 1.

Table 1: *Essential geometric data*

Quality	Size
weight	11kg
sweep angle	22°
washout twist angle	3°
span	3048mm
aspect ratio	8.4
chord length	295mm

Figure 2: *The A3TB with a dog for scale*

ii. Finite-element model

Based on the shown geometry, a finite element (F.E.) model was built using FEMAP. The F.E. model, as shown in Figure 3, was used in a free vibration analysis by the Nastran program. The model have 13981 nodes, and 15670 elements.

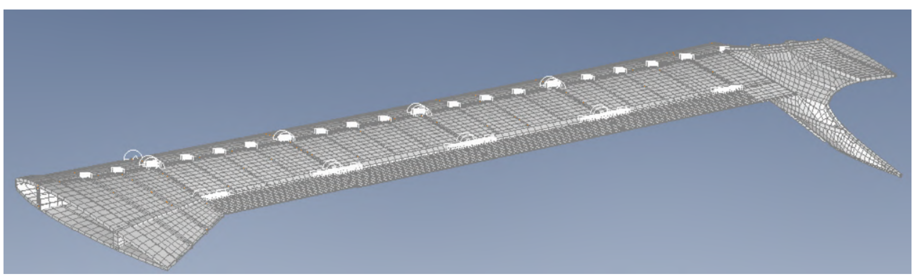

Figure 3: *The finite element model of the A3TB wing*

ii.1 Basic elements in the F.E. model

The main spar of the wing is made of the carbon beam which acts as a web and the PA12 sleeve in which it is inserted (see figure 4) which acts as the flanges. The carbon beam is modeled as a laminate plate. The segments are connected to each other via a rigid connection in selected places, as shown in Figure 5. The rear spar of the wing, to which the control surfaces attach (shown in figure 6) is modeled as a beam (figure 7). The leading edge (L.E) spar, the ribs, and the flaps hinges, are also represented by beam elements. The fin (figure 8) is represented by its geometrical form with beam elements and plate elements. Due to modeling considerations, a new material card was designed in order to model the fin, with density close to the PA12 but double the stiffness (see figure 9). The upper and lower surfaces of the fin (see figure 8, left) were modeled with plates and the rest of it modeled as beams.

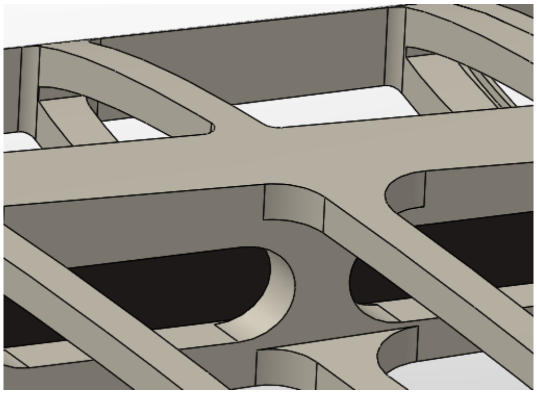

Figure 4: *A segment with the carbon beam (black) inserted*

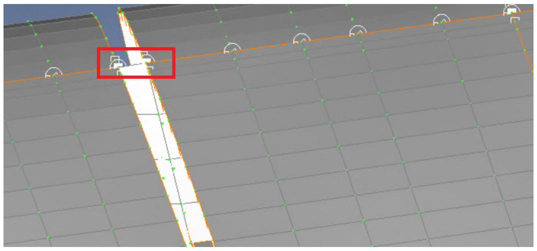

Figure 5: *A view of the connection made between two segments in the finite element model*

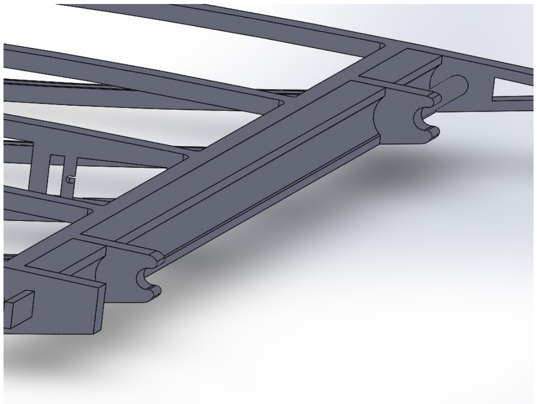

Figure 6: *rear spar in CAD model*

The wings' root (Figure 10) is modeled with plate elements for the profile, the rest as beams. The ribs of the root are modeled with different (thicker) cross section compared to those of the wing, but the material is the same (PA12).

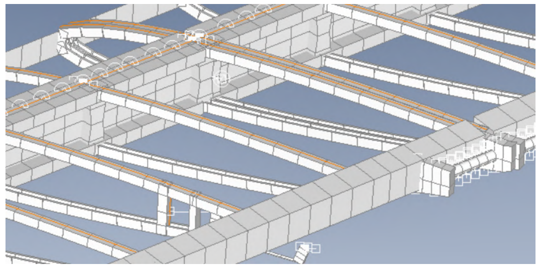

Figure 7: *The rear spar in FEM model*

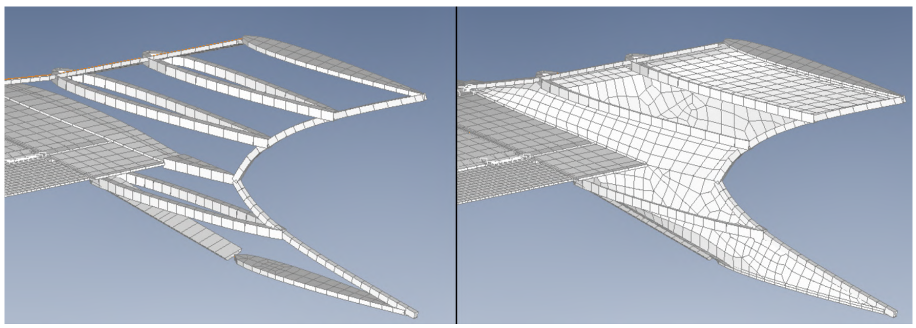

Figure 8: *Left: fin without the skin, Right: fin with skin*

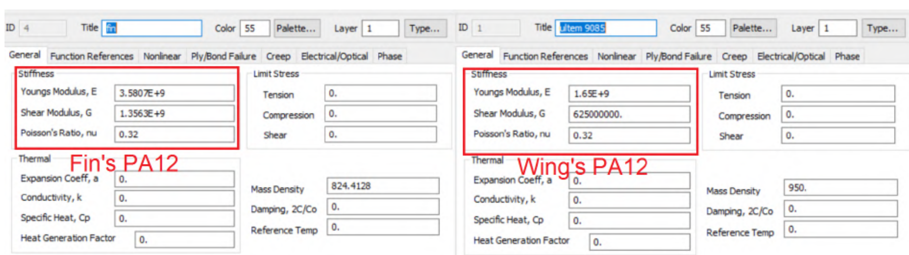

Figure 9: *Material cards of the fin and wing*

The wing's flap (Figure 11) is modeled with plates, the flaps are connected to the main wing body with rigid (RBE2) connections in translation and spring (CBUSH) connections.
The flap's hinge (Figure 12) is modeled withe cylindrical beam, between two knobs that keep the joint in place. The flap is connected to the rear spar via a beam with a circular cross-section that represents the servo's push-rod.

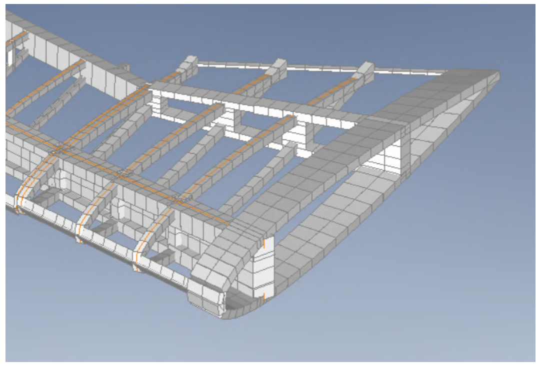

Figure 10: *Wing root section in the F.E model*

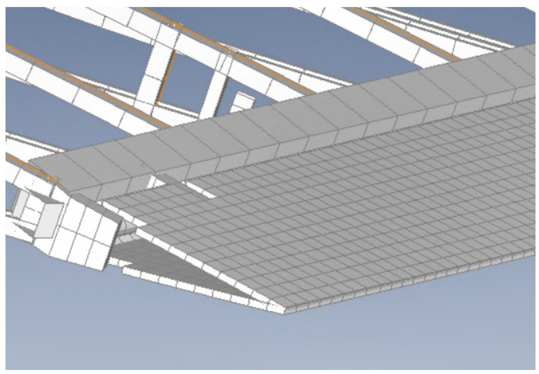

Figure 11: *Wing's flap in the F.E model*

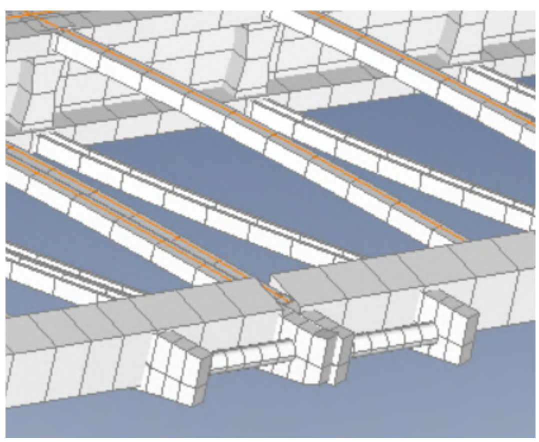

Figure 12: *Flap's hinge in the F.E model*

ii.2 Connections between elements

As shown in figure 13 in yellow, the model has many rigid connection within it. The main connection and their purposes are:

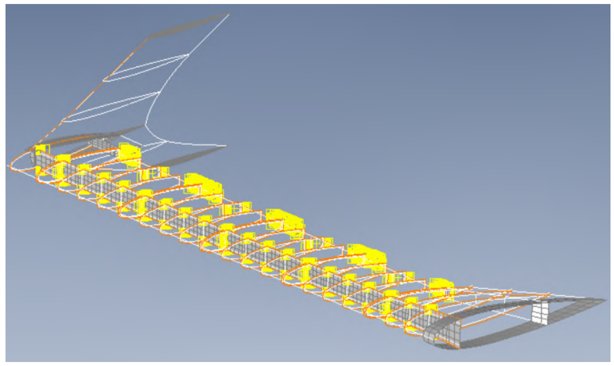

Figure 13: *Rigid connections in the model (yellow)*

1) Flaps: In figure 14 we see how the hinge is connected with the flap via a rigid connection in all DOFs from the flap to springs along the hinge that have no rotation stiffness, s.t the hing and the flap are connected. Rotation is allowed thought the connection between the knob and the hing, where there is a rigid connection only in the translation DOFs. In the right side of figure 14 the flap connection to the hinge is shown, in the left side the same connection is shown but without the flap itself, where the hinge is the white line with the filled yellow squares on it. The yellow filled squares is the source nodes of the rigid connection.

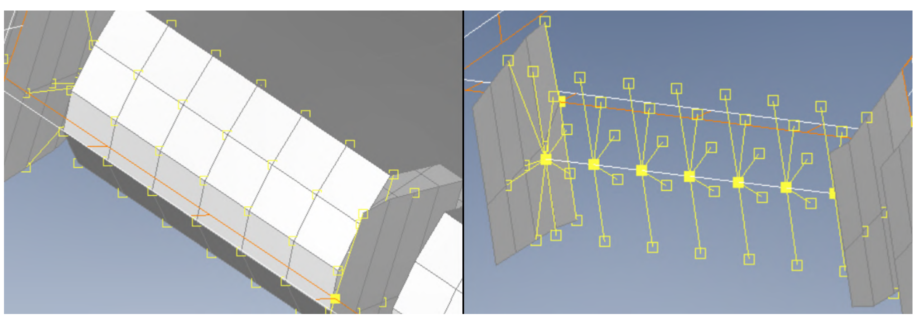

Figure 14: *Rigid connection between flaps and hinge*

2) Segments connection: The connection between every two wing segments, modeled with two groups of rigid-connected nodes at each side, and the two groups connected via a spring with stiffness at all DOFs.
3) Rib-main spar connection: the wing segments are threaded on the main spar and fit there snugly. To model this, the main spar and the ribs were connected with rigid connection at the contact points, on the upper and lower surfaces.
4) Servo and flap: The connection between the servo and the flap was modeled as a beam (servo rod) that connects the servo and flap via a rigid connection at the edges.

Spring connections: The model have spring connections (see in green in figure 15) modeled with CBUSH elements. The main connection and their purposes are:
1) Segments joiner: As described in the rigid connection section, the wing's segments are connected between each other trough a spring with stiffness in all DOFs.
2) Flaps: As described in the rigid connection section, the flaps are connected to the hinge through spring connection with stiffness only in the translation DOFs to allow rotations.
3)The main-spar: The main spar is connected to its sleeve with a spring, which allows slip in the span direction, and have stiffness in all the other DOFs.

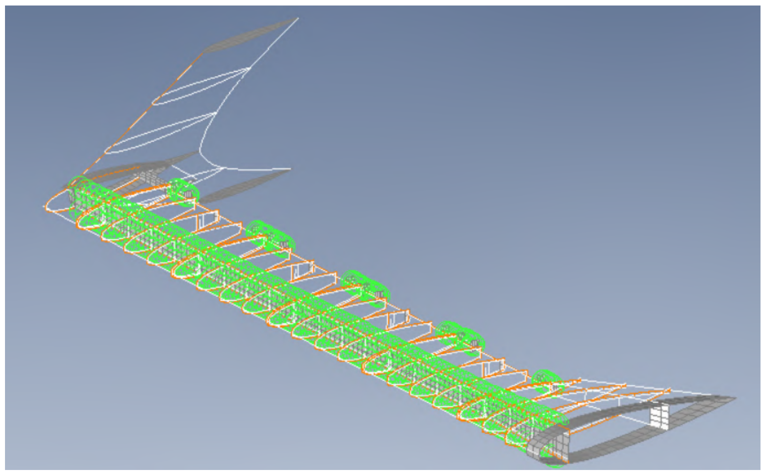

Figure 15: *Spring connections in the model (green)*

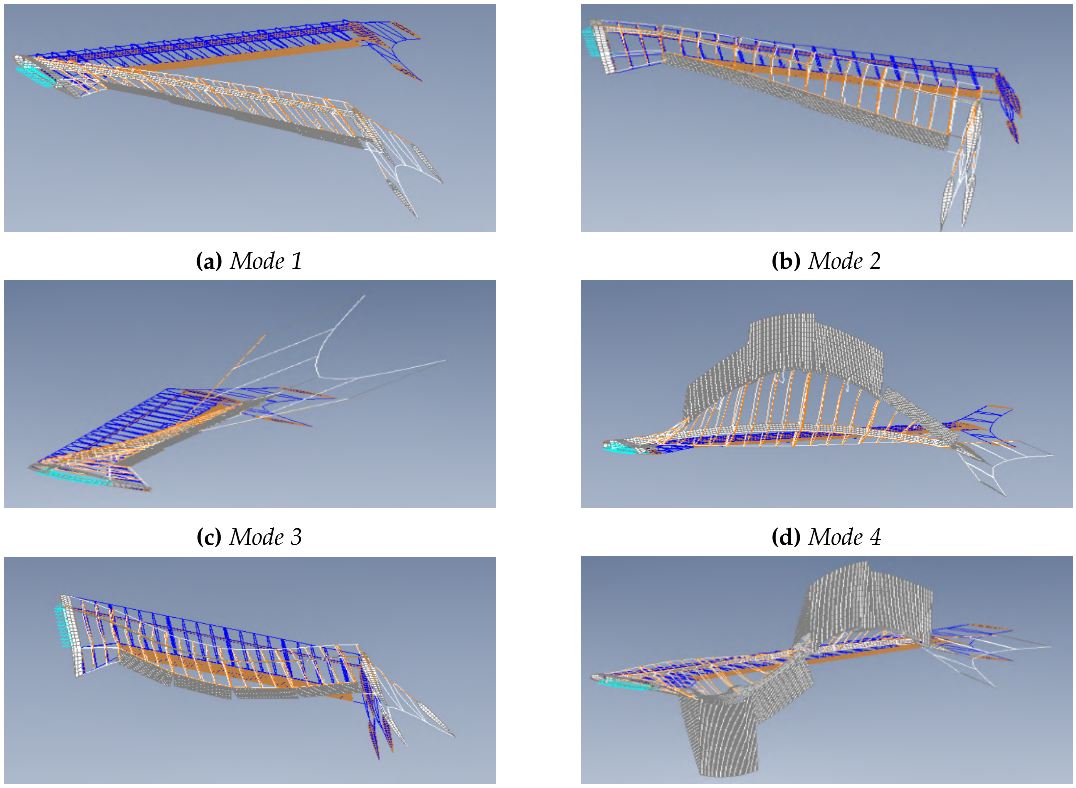

(a) *Mode 1* **(b)** *Mode 2*

(c) *Mode 3* **(d)** *Mode 4*

(e) *Mode 5* **(f)** *Mode 6*

Figure 16: *Modes of the F.E model*

IV. Free vibration analysis

The free vibration analysis was made for the clamped model. Table 2 provides the first six modes and their frequencies. The modes are shown in figure 16.

Table 2: *Modal analysis results*

Mode	Frequency (Hz)	Description
1	2.9	First bending
2	7.5	Chordwise first bending
3	8	First torsion
4	18.8	Second Bending + torsion
5	28.5	Second chordwise bending
6	29.9	Third bending

V. Flutter analysis

The flutter calculations were done with the ZAERO software and by using the k and g methods. ZAERO uses a linear panel method [5], in which every aerodynamic surface is divided into aerodynamic panels in the chordwise and spanwise directions. In the aerodynamic model, the wing is represented by four surfaces: root, wing, upper part of the fin and the lower part of the fin. Figure 17 shows the four surfaces. Table 3 provides the number of spanwise and chordwise segmentation of the surfaces. The structural modes mapped to the aerodynamic model appear in figure 18. The flutter analysis (figure 19) shows an ω-v-g plot, describing the frequency and

Table 3: *Aerodynamic model*

Element	Chordwise boxes	Spanwise boxes
Wing root	19	13
Wing	19	35
Fin - upper	6	6
Fin - lower	6	6

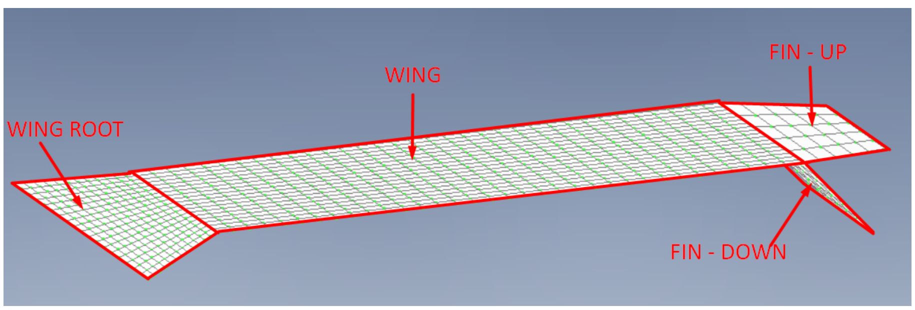

Figure 17: *Aerodynamic model from ZAERO*

damping of the aeroelastic modes with flight speed. Flutter was computed at 16.5[m/s] (32[knots]) which is inside the flight envelope. And divergence at 26.2[m/s] (50.9 [knots]). The flutter speed was calculated for zero structural damping. The flutter frequency is 6.6Hz. The flutter mode, shown in figure 20, is mainly torsion coupled with first bending.

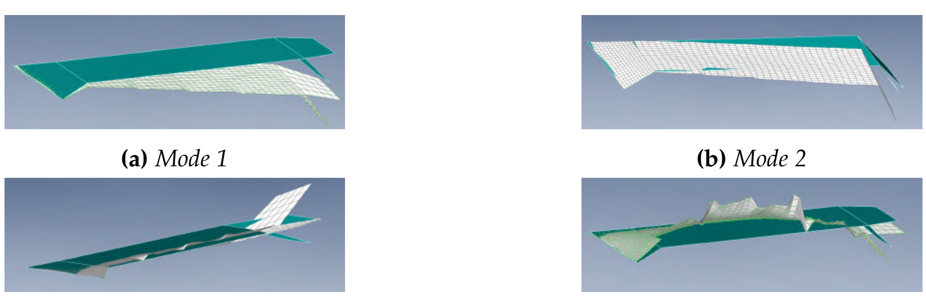

(a) *Mode 1* **(b)** *Mode 2*

(c) *Mode 3* **(d)** *Mode 4*

Figure 18: *Modes mapped to the aerodynamic model*

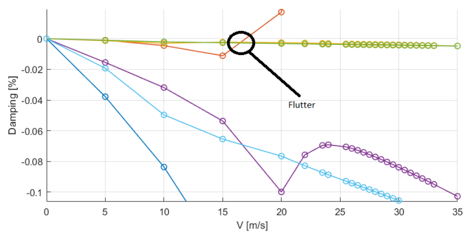

(a) *damping VS speed*

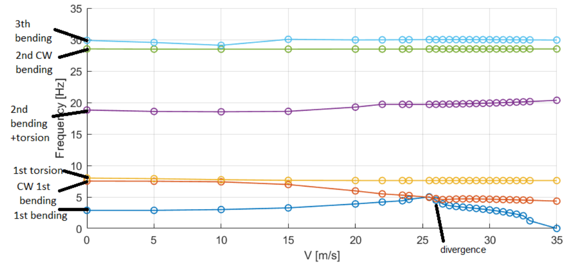

(b) *frequency VS speed*

Figure 19: *ω-v-g plot*

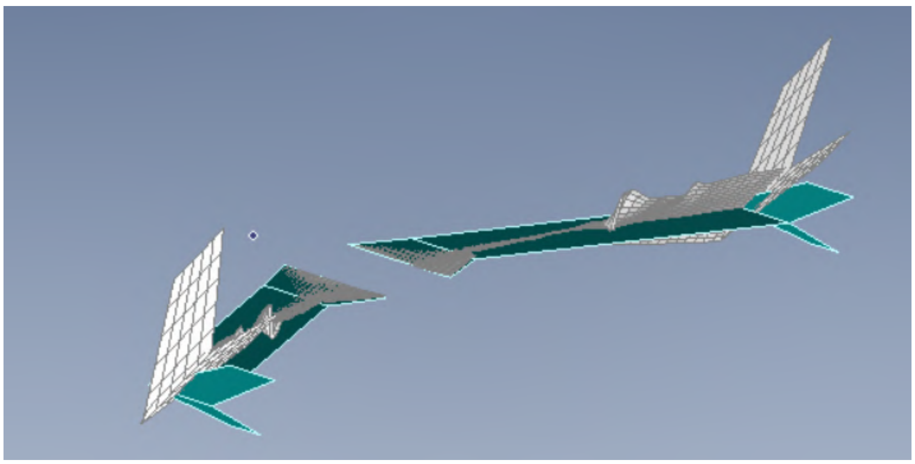

Figure 20: *Flutter mode - 6.6Hz*

VI. Passive means for increasing the flutter speed

Due to the presence of flutter inside the flight envelop, the possibility of passive means to postpone the flutter onset was investigated. The solution that was examined is addition of a weight to the leading edge of the wing.
Two locations of the weight were investigated: center and tip of the wing at the leading edge (see figures 21 and 22 respectively). For each location, a set of weights with masses between 0 to 600gr in 100gr steps was examined. The weights were modeled as a concentrated mass (CONM element), which have only mass and no inertia properties.

Figures 23 and 24 present the flutter onset speeds with added weights at the center-span and wingtip respectively. It is seen that flutter speed can be increased with mass addition to the leading edge of the wing, and that adding mass to the leading edge tip is more effective, but with a limit of 400gr.

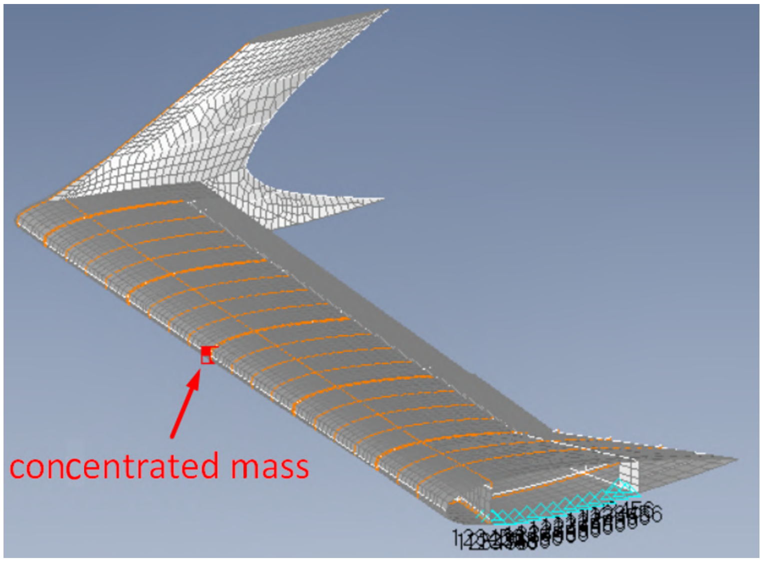

Figure 21: *Concentrated mass location on model*

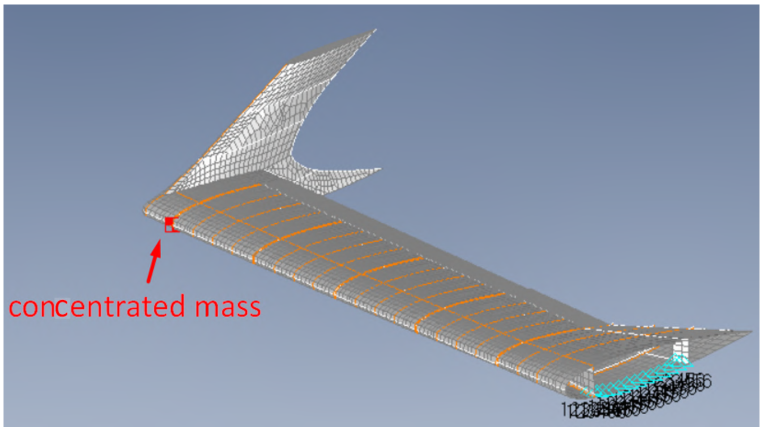

Figure 22: *Concentrated mass location on model*

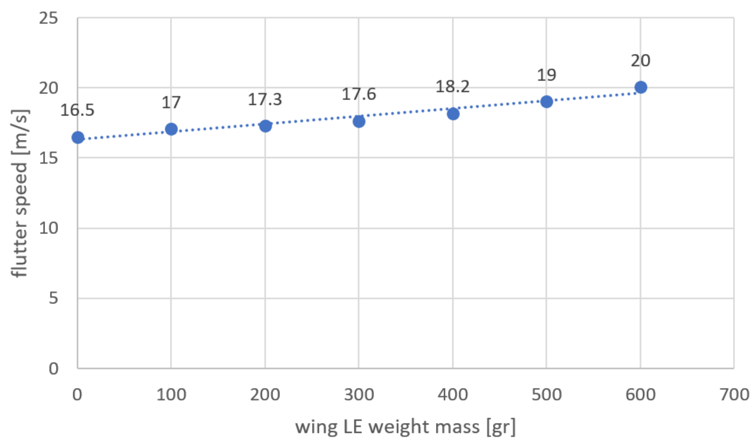

Figure 23: *Flutter analysis results with concentrated mass at the center of the wing*

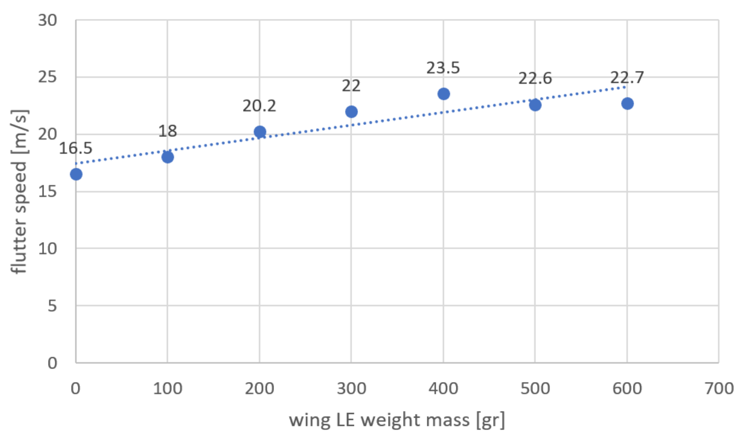

Figure 24: *Flutter analysis results with concentrated mass at the tip of the wing*

VII. Conclusions

Flutter analysis of the clamped configuration indicated that the aircraft is vulnerable to flutter inside the flight envelope. The flutter mode is a combination of torsion with bending of the wing. Increasing the flutter to higher significant speeds require a large weight addition and therefore might increase the total aircraft weight significantly. For example, the addition of 400gr in the wingtip will improve flutter speed by about 7[m/s]. Further study is needed for flutter predictions of the aircraft including rigid modes. This will give a more realistic prediction of the A3TB aeroelastic stability.

References

[1] C. E. Cesnik, R. Palacios, and E. Y. Reichenbach. Reexamined structural design procedures for very flexible aircraft. *Journal of Aircraft*, 51(5):1580–1591, 2014.

[2] M. Love, P. Zink, P. Wieselmann, and H. Youngren. Body freedom flutter of high aspect ratio flying wings. In *46th AIAA/ASME/ASCE/AHS/ASC Structures, Structural Dynamics and Materials Conference*, page 1947, 2005.

[3] J. J. Ryan and J. T. Bosworth. Current and future research in active control of lightweight, flexible structures using the x-56 aircraft. In *52nd Aerospace Sciences Meeting*, page 0597, 2014.

[4] J. Theis, H. Pfifer, and P. J. Seiler. Robust control design for active flutter suppression. In *AIAA Atmospheric Flight Mechanics Conference*, page 1751, 2016.

[5] ZONA. *ZAERO theoretical manual*. ZONA Technology Inc, 2016.